Evaluation of An Erbium-Doped Fiber Ring Laser, as An Edge Filtering Device for FBG Sensor Interrogation

Nikolaos A. Stathopoulos *, Christos Lazakis, Iraklis Simos, Christos Simos *

Posted Date: 8 April 2024

doi: 10.20944/preprints202404.0491.v1

Keywords: fiber bragg gratings; erbium-doped optical fibers; fiber optic sensors

Article

Evaluation of an Erbium-Doped Fiber Ring Laser, as an Edge Filtering Device for FBG Sensor Interrogation

Nikolaos A. Stathopoulos [1,*], Christos Lazakis [1], Iraklis Simos [1] and Christos Simos [2,*]

[1] Department of Electrical and Electronics Engineering, University of West Attica, 12244 Aegaleo, Athens, Greece
[2] Electronics and Photonics Laboratory, Department of Physics, University of Thessaly, Lamia, Greece
* Correspondence: nstath@uniwa.gr (N.A.S.); christos.simos@uth.gr (C.S.)

Abstract: An easy to implement and cost-effective Fiber Bragg Grating (FBG) sensor interrogation technique based on a ring Erbium-Doped Fiber Laser (EDFL) topology is proposed and experimentally assessed. The FBG sensor is part of the EDFL cavity and must have a central wavelength located within the linear region of the EDF's amplified spontaneous emission (ASE) spectrum which occurs between 1530 and 1540nm. In this manner, the wavelength-encoded response of the FBG under strain is converted to a linear variation of the laser output power, removing the need for spectrum analysis as well as any limitations from the use of external edge-filtering components. In addition, the laser linewidth is significantly reduced with respect to the FBG bandwidth thus improving the resolution of the system, whereas its sensitivity can be controlled through the pumping power. The performance of the system has been characterized by modeling and experiments for EDF's with different lengths, doping concentrations and pumping power levels. The influence of mode-hopping in the laser cavity on the resolution and accuracy of the system has also been investigated.

Keywords: Fiber Bragg Gratings; erbium-doped optical fibers; fiber optic sensors

1. Introduction

Strain and structural health monitoring systems are increasingly used for infrastructures and constructions with high standards and strict specifications. The state of the art of these systems utilizes complicated and sophisticated fiber optic sensor techniques in order to monitor the increased number of sensing points [1,2]. Most of them require sequentially located FBGs with different central wavelengths, while their interrogation systems are mainly based on either tunable lasers or spectrum analyzers [3–5] which are in general high-end and high-cost components.

On the other hand, there are also many small-scale applications that require a small number of FBG sensors where cost and simplicity are the most significant requirements. For these applications, alternative lower cost systems are required. A potential interrogation method could use a time division multiplexing topology, consisting of FBGs with similar center wavelengths inscribed on different fibers and polled by means of an optical switch. Then, a single channel interrogator is required and may be based on an edge-filtering component matched to the FBG wavelength range that transforms the wavelength-encoded strain or temperature response of the FBG into power variation [6,7].

Edge filters are usually implemented either by biconical fibers [8] or by means of chirped and apodised grating inscriptions on the fiber core and therefore require a rather complicated design [6,9,10]. In addition, they exhibit a limited linear spectral response up to 2nm that remains unchanged, unless their temperature is varied through a temperature control system. Edge filters for FBG interrogation based on unpumped erbium doped fibers (EDFs) have also been proposed [11,12]. They exploit the linear region of the absorption spectrum of the EDF and in general suffer from low output power levels.

 doi:10.20944/preprints202404.0491.v1

In the present work we propose and evaluate an FBG interrogation technique that relies on an erbium doped fiber laser (EDFL), in a well-known ring cavity configuration which includes the strain sensing FBG. The novelty of the proposed technique is that the FBG sensing element must exhibit a central reflectivity wavelength within the 1532-1537 nm wavelength range, where the ASE spectrum of Erbium exhibits an abrupt slope. By means of the combination of a ring EDFL cavity with this specific FBG, any strain-induced wavelength shift of the FBG, not only shifts the laser wavelength, but also induces a linear variation of the laser power, due to the abrupt variation of the EDF-ASE spectrum within the above wavelength range. Thus, the proposed topology behaves like an edge filter, eliminating the need for spectrum analysis or external linear edge-filtering components, that are commonly used in typical power-detection interrogation systems [13]. Therefore, the proposed topology is simpler, reducing complexity and cost, while at the same time extends the linear range of operation to more than 3nm covering many possible sensor variations. In addition, the ring laser topology provides higher power compared to the unpumped EDFs that are used for edge-filtering and also reduces the output half-power bandwidth, offering higher resolution. Furthermore, by embedding a 1×N optical switch, the proposed topology may be connected to several identical sensors [14] in order to evaluate multiple sensing points and temperature-reference sensors.

The paper is organized as follows: Section 2 comprises the system principle of operation and a theoretical investigation by means of a numerical model for validation of the principle and specific case studies. Section 3 describes the experimental setup and characterization of the most significant components. Finally, in Section 4, the operation of the device as a strain sensor interrogator is fully characterized and analyzed considering potential applications requirements.

2. Principle of Operation

The proposed interrogation technique exploits the quasi-linear slope of the amplified spontaneous emission (ASE) of an erbium doped fiber (EDF), in a narrow spectral range between 1532 and 1537nm and is explained with the sketch of Figure 1. The EDF is used as the gain element of a ring laser cavity which also includes the FBG that will be used as a strain sensing element. The FBG is connected to the cavity by means of a circulator and is chosen so that its central wavelength to be in the linear region of the EDF emission (1532-1537 nm) and therefore determines the central emission wavelength of the laser.

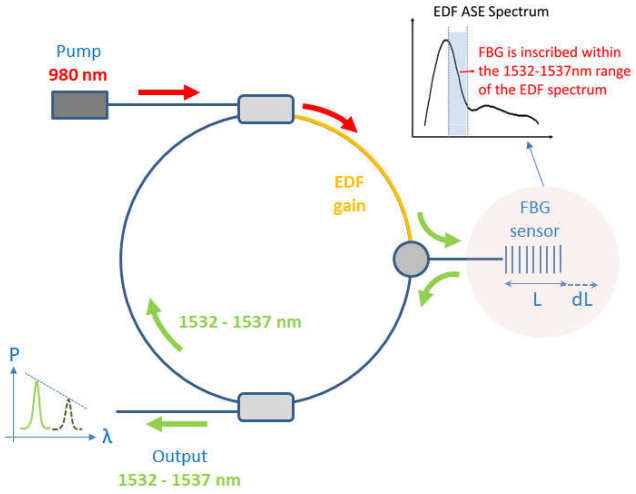

Figure 1. Illustrative presentation of the unidirectional EDFL based FBG sensor interrogation system.

Any strain or temperature induced wavelength-shift of the FBG, shifts the laser emission wavelength as well, and induces a linear variation of the cavity gain and therefore a linear variation of the laser output power. Therefore, the wavelength-encoded strain or temperature response of the FBG is transformed into a laser power variation which can be trivially measured with a photodiode.

 doi:10.20944/preprints202404.0491.v1

In this manner the system behaves similarly to an edge filtering device, without the main drawbacks of edge filters.

In order to verify that the system will exhibit a linear response for EDF's with different doping concentrations, lengths and pumping levels, we performed simulations based on the numerical model that is described in the Appendix A herein. The model is based on gain saturation models for EDFs [15–19] including the pair-induced quenching phenomenon for high doping concentration [20–22] and fitting of unknown parameters with experimental results. It is noted that only high-doping EDFs have been used, to keep their length short and at the same time provide sufficient small-signal gain.

The model provides an efficient way to calculate steady state values of critical parameters for the ring-laser topology of Figure 1 (e.g. saturated gain and output power) assuming single-pass amplification of a signal through an EDF with specific characteristics. Each value of the EDF input power considered in the model, corresponds to a value of the saturated optical power circulating in the EDFL cavity of Figure 1.

A typical simulation result is presented in Figure 2 and shows the calculated EDF gain versus the input signal power of five different wavelengths, for a 62cm long Er30 EDF with a pumping level of 60mW. From this diagram, the output power of the EDFL sketched in Figure 1, at each wavelength can be extracted straightforwardly, since it is equal to the input power value for which the loop gain of the ring cavity compensates the loop losses. The specific example shown in Figure 2 assumes 7.65dB of total loop losses in the EDFL ring cavity (horizontal dashed line) according to the experimental setup of Section 3, and results in output power levels marked with the vertical dashed lines. As clearly shown in the inset of Figure 2, the laser output power varies linearly with wavelength, leading to a linear system response.

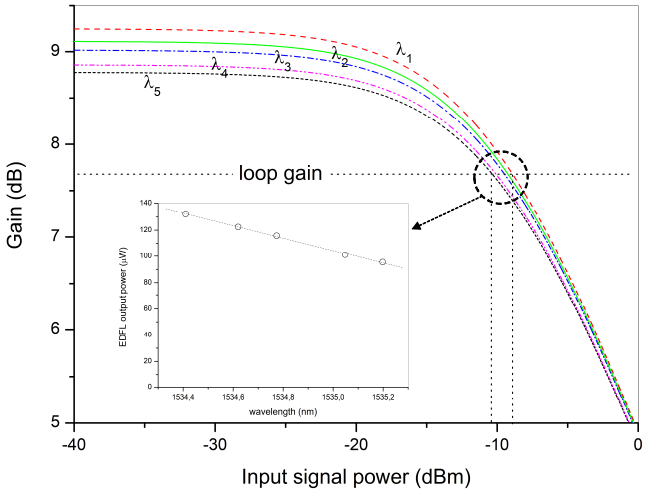

Figure 2. Calculated gain saturation versus the input signal power for five different wavelengths for a 62cm Er30 EDF with 60mW pump power. Considering 7.65dB loop gain, the input signal is calculated for each wavelength and depicted in the inset. For the wavelength values of λ_1 to λ_5 see also Figure 9.

In addition, the aforementioned model was used to provide some design rules with respect to setup parameters such as the EDF's doping, length and the pumping power, that affect the ring-laser's output power.

Figure 3 presents a calculation example with a higher doped EDF (Er110). The EDF gain is plotted versus the input optical signal power for two lengths of 40cm (solid lines) and 47cm (dashed lines) and two pumping levels of 75mW (blue lines) and 90mW (red lines). For input power higher than -25 dBm, the EDF length does not provide any significant gain difference. On the contrary, the pumping level (75 or 95mW) affects gain significantly. Regarding the doping concentration of the two EDFs, there is no clear choice between the two examined. Lower doping requires a relatively

 doi:10.20944/preprints202404.0491.v1

longer length and less pumping, although it provides less small-signal-gain which makes the laser ignition more difficult. In any case there is a tradeoff between the loop losses, the EDF doping and length, together with the required pumping power.

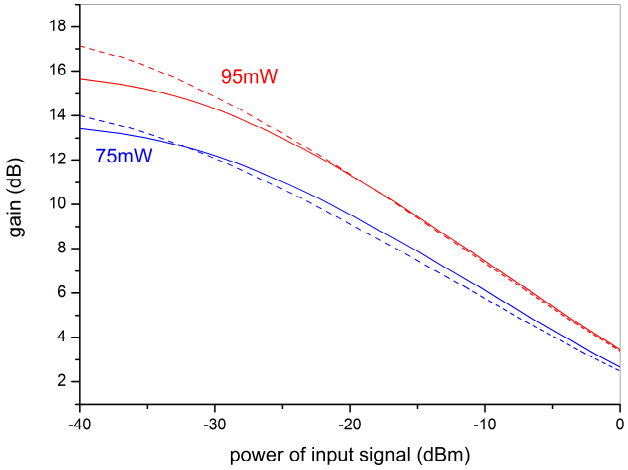

Figure 3. Calculation of gain saturation vs the input signal power for an Er110 EDF with length of 40cm (solid lines) and 47cm (dashed lines) and a pumping power of 75mW (blue lines) and 95mW (red lines).

3. Experimental Setup

The experimental setup used for the proof of concept of the proposed interrogator is sketched in Figure 4. The EDF is part of a unidirectional ring laser cavity and is pumped at 975 nm by a laser diode (LD-Thorlabs PL980P330J) through a WDM combiner. An optical circulator imposes unidirectional operation whereas a fiber splitter sends a fraction of the cavity power to a photodiode for measurement of the laser power or to a Spectrum Analyzer for monitoring the wavelength shift. The strain sensing FBG is chosen so that its central wavelength is in the quasi-linear region of the EDF ASE emission (1532-1537 nm) and is connected to the cavity by means of the circulator, thus reflecting part of the cavity signal power back in the cavity.

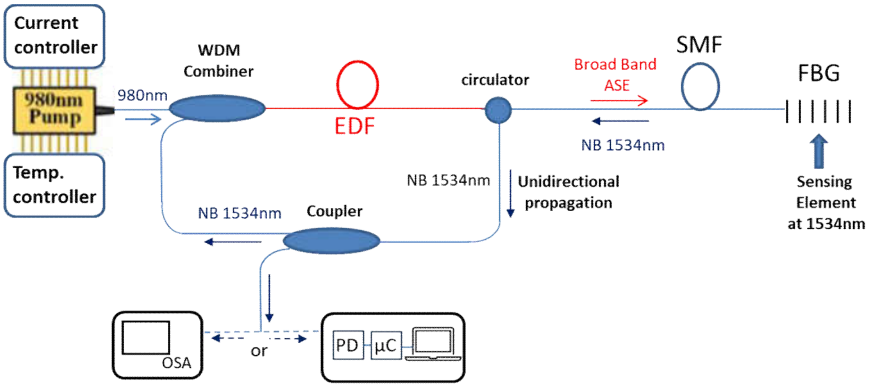

Figure 4. Experimental setup of the FBG interrogator. PD: photodiode, µC: microcontroller, OSA: optical spectrum analyzer, EDF: erbium doped fiber.

Considering the required strain-induced wavelength-shift of the FBG for structural health monitoring applications together with the width of the quasi-linear slope of the EDF, the FBG sensor for optimal operation should be inscribed with a central wavelength close to the center of the above region, that is close to 1534nm and with an optimal bandwidth of 1-3nm.

 doi:10.20944/preprints202404.0491.v1

Since the laser power is expected to exhibit a linear response to the wavelength shift of the FBG for fibers of different doping concentrations as mentioned in the previous section, for the experimental demonstration we used a heavily doped single-mode fiber (Er110, nLIGHT) with an Erbium-ion concentration of 6.6×10^{25} ions per m^3. The high Erbium-ion concentration has been adopted in order to reduce the required length of the EDF while at the same time the high small signal gain will compensate the loop losses, as mentioned in the analysis of Section 2.

The FBG of Figure 4 was inscribed in house, using a UV laser emitting at 266nm, a phase mask with 1060nm pitch and a GF1 as photosensitive fiber. Figure 5 shows the power reflectivity spectrum of the inscribed FBG (red solid line), together with the theoretically calculated response (black dashed line) [23]. The FBG exhibits a peak power reflectivity of about 48% at a center (Bragg) wavelength of λ_B=1534.1nm and with a 1dB bandwidth of about 80pm. The length of the FBG is approximately 6mm.

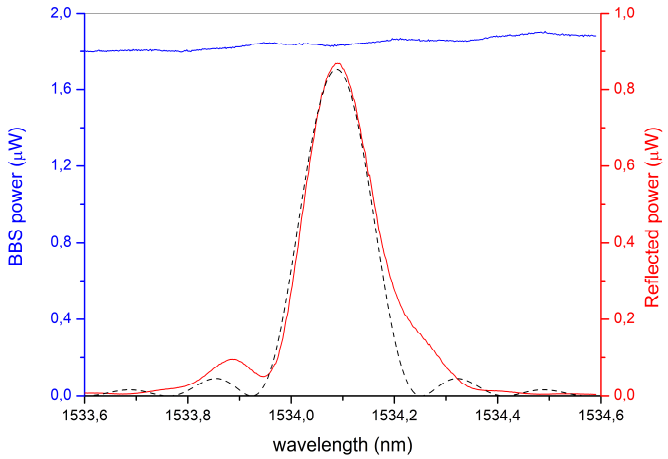

Figure 5. Spectral reflected power from the FBG (red solid line), together with the broadband source (BBS) power spectrum (blue solid line) and FBG's calculated spectral reflectivity (dashed black line).

Figure 6 depicts the spectrum of the ring laser for 75mW of pumping power (solid blue line), along with the FBG bandwidth (solid red line). The laser power at the peak wavelength of 1534.1nm is approximately 23μW which is in a good agreement with the -16dBm value predicted by the model for 8.2 dB cavity loss (3.2dB of FBG reflectivity and 5dB residual loop losses) and 75mW of pumping power (see Figure 3). Furthermore, the laser exhibits significantly narrower spectrum compared to the FBG reflectivity bandwidth (20pm and 80pm bandwidth at -1dB, respectively). The narrow linewidth together with the high output power, lead respectively to improved resolution and lower noise floor for FBG sensing applications, compared to systems that rely on other types of edge filters.

 doi:10.20944/preprints202404.0491.v1

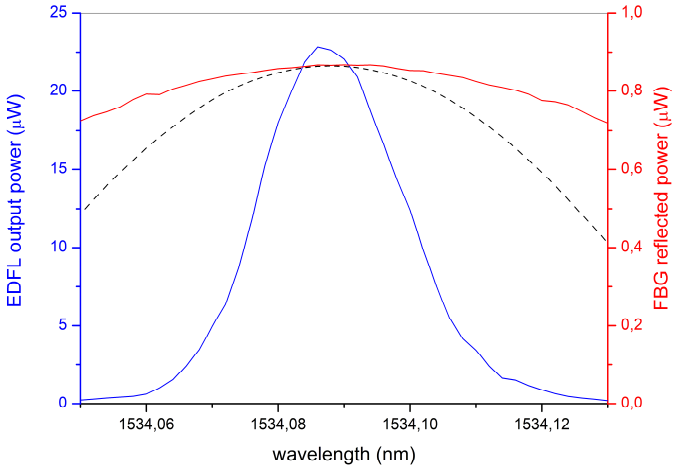

Figure 6. Spectral output power of the ring-EDFL for 75mW of pumping power (solid blue line), together with the FBG's power-reflection spectrum (solid red line) and a calculated example of a narrower uniform FBG (dashed line) that is proposed in order to reduce mode hopping.

Nevertheless, this family of long cavity EDF ring lasers exhibits strongly multi-longitudinal mode spectrum and suffers from the mode-jumping (or mode-hopping) phenomenon which causes wavelength and optical power instability [24,25]. In our case mode-hopping limits the resolution of the FBG interrogation and needs to be addressed. To tackle this problem, a much narrower FBG with reflectivity less than 50% should be used, in order to act as a narrowband filter. An example is depicted in Figure 6 (dashed line), which could limit mode jumping in a range of approximately 20pm around the center wavelength without significant variation of the laser power. This FBG can be implemented by increasing the inscription length of the grating and reducing the index modulation depth at the same time.

4. Characterization as a Strain Sensor Interrogator

In a last step we evaluate the proposed technique as a strain sensing interrogator, using the setup of Figure 7. By applying a variable strain up to 1200με to the FBG sensor, its center wavelength is red-shifted by more than 1nm and we record the laser power at the peak wavelength using a spectrum analyzer, for two pumping levels of 75mW and 95mW (see Figure 8). The power versus wavelength-shift sensitivity ($dP/d\lambda$) of the device, increases with the pumping level (8.8μW/nm to 11.6μW/nm for 75mW and 95mW pumping respectively) and consequently, the strain sensitivity increases from 1.38μW/100με to 1.79μW/100με for 75mW and 95mW pumping. Moreover, for both pumping levels, the system response remains linear while any small fluctuations are mainly due to noise and residual mode-hopping effects. Finally, the dynamic range of the system is also affected by the pumping level since higher pumping leads to increased laser power and therefore larger dynamic range before approaching the noise floor of the photodetector. Specifically, for our experimental conditions the dynamic range for a pumping level of 75mW was approximately 1300με, while for 95mW the dynamic range exceeds 2000με. The above results show that the pumping power affects critically both the resolution and the dynamic range of the proposed technique.

Preprints.org (www.preprints.org) | NOT PEER-REVIEWED | Posted: 8 April 2024 doi:10.20944/preprints202404.0491.v1

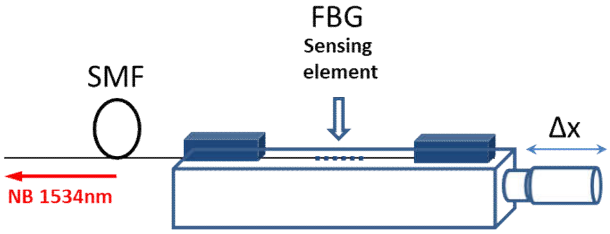

Figure 7. One-dimensional stage for the axial elongation of the FBG element.

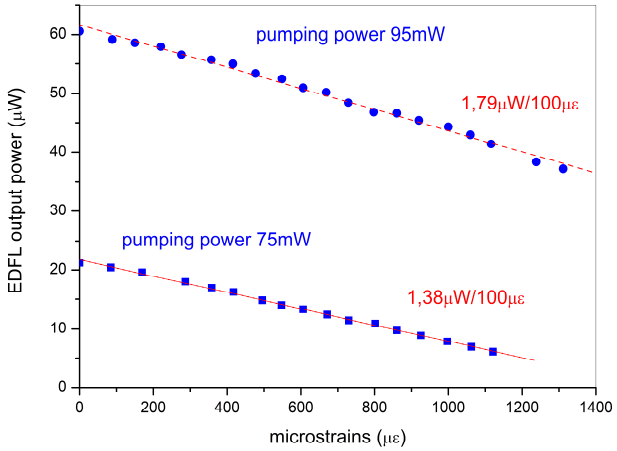

Figure 8. Output power of the ring EDFL vs strain applied on the FBG, for 75mW (square dots) and 95mW (round dots) of pumping power of the Er110 EDF, together with linear fitting.

Similar results were obtained with a 62cm long EDF with lower doping concentration (Er30). Figure 9 shows the laser power at the peak wavelength as recorded with the optical spectrum analyzer, for various strain levels and a pumping power of 60mW. Squares represent the calculated power values at the corresponding peak wavelengths, using the numerical model of the Appendix and considering a cavity loss of 7.65dB (see also the inset of Figure 2). We remark again the linear response of the output power to the strain induced wavelength shift as well as the good agreement between experimental and theoretical results. The sensitivity in this configuration example increases up to 7,22μW/100με due to the higher output power in comparison with the Er110 EDF.

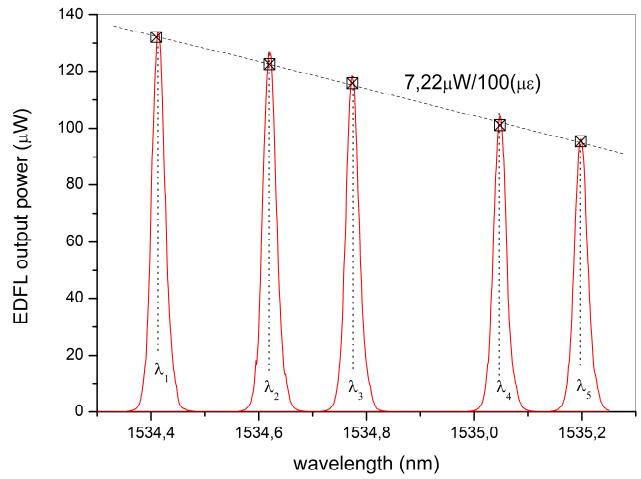

 doi:10.20944/preprints202404.0491.v1

Figure 9. Ring – EDFL emission spectra for Er30 EDF and 60mW of pump power (red solid lines). The square symbols represent the corresponding theoretical calculation for each wavelength while the linear fitting gives sensitivity of 7,22μW/100(με).

Furthermore, a photodiode with an analog to digital converter (ADC) have been employed, in order to evaluate the accuracy and the resolution of the proposed method. With the previously used Er30 EDF, we plotted the output voltage versus the axial strain in Figure 10 (red data). For a strain range up to 1000με, the sensitivity is approximately 200mV per 100με (R^2=99.31%). However, we remark a fluctuation in sensitivity of approximately ±2.5% which limits the resolution to approximately 20με, which may fulfill applications with loose specifications and is mainly caused by mode-hopping. Improvement of the resolution is expected by a narrower FBG, as was discussed in the previous section. In order to experimentally confirm this assumption, a 25% narrower FBG was used (inscribed in house with a slight increase of the inscription length and a small reduction of the peak reflectivity). The corresponding results are depicted in Figure 10 (blue data). The calculated sensitivity is now 270mV per 100με (R^2=99.79%), while the maximum fluctuation in sensitivity is less than 2% which leads to a resolution better than 15με. This improvement is mainly provided by the reduction of mode hopping due to the respective reduction of the FWHM bandwidth. Further reduction of the FBG bandwidth will improve the strain resolution and accuracy of the method down to the limit imposed by the stability of the pump power.

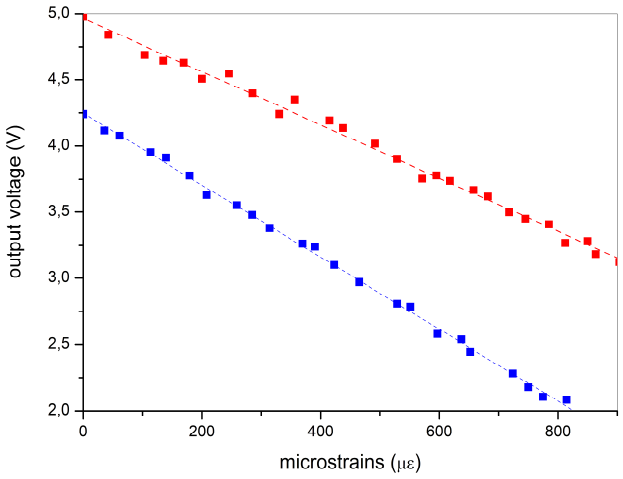

Figure 10. The output voltage of an ADC that reads the photodiode's photocurrent, versus the axial strain applied on the FBG in microstrains. The red dotted line is the linear fitting for the measured data (square dots), while, both the blue line and the blue square dots represent the measured data from a narrower FBG together with their linear fit.

Finally, we evaluated the sensitivity of the system to the environmental temperature changes. This is a crucial parameter for sensing applications because, due to the thermo-optic effect, temperature is expected to affect both the reflectivity and the peak wavelength of the FBG. Specifically, the FBG (Bragg) wavelength increases with temperature, while reflectivity decreases due to the change of the material refractive index. Both parameters, will lead to change of the output power of the device, which can be falsely translated to strain originating changes. In order to assess the temperature sensitivity of the device, we varied the FBG temperature keeping strain constant, and we recorded the output spectra for several temperatures.

The results are depicted in Figure 11 which shows that the temperature sensitivity is almost 2μW per 10°C. Therefore, due to the high temperature sensitivity, strain-sensing applications require a dummy (strain-free) identical FBG as a reference for temperature compensation. The reference FBG will be used not only to compensate the temperature variations, but the pumping power

 doi:10.20944/preprints202404.0491.v1

fluctuations as well. Moreover, the LD's output power could be monitored and corrected accordingly, through the adequate controller's software. Nevertheless, each sensor's calibration procedure, together with its reference-FBG, should be conducted individually, in order to determine the strain and temperature sensitivity.

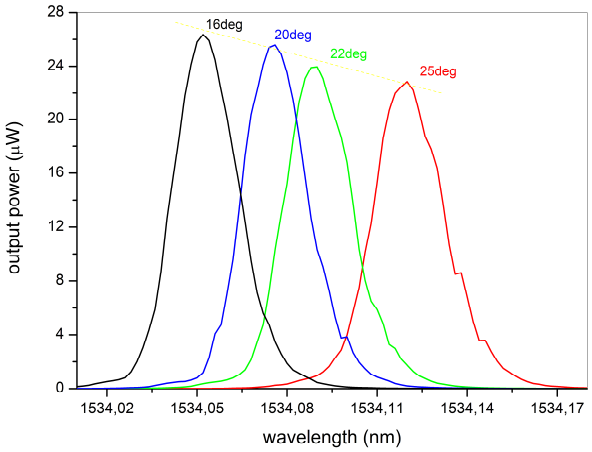

Figure 11. Ring – EDFL topology emission spectra for 75mW pumping power, without any strain on the FBG and for temperatures from 16 to 25 °C.

5. Conclusions

An FBG sensor interrogation technique suitable for low cost and small-scale sensing applications has been proposed. The interrogator is based on an EDFL in a ring cavity configuration which comprises the FBG sensor as part of the cavity. The proposed configuration transforms the strain or temperature induced wavelength shift of the FBG into variation of the laser power, relying on the slope of EDF ASE between 1532 and 1537 nm, provided that a sensor with a central wavelength within this range is used. The topology has been evaluated for an FBG with center wavelength of 1534.1 nm for several pumping powers and different EDF types and lengths. It is demonstrated theoretically and experimentally that for strain-induced wavelength shifts of the order of 1-3 nm which are sufficient for structural health monitoring applications, the laser power varies linearly with wavelength, thus leading to a linear system response. The main advantages of the technique include the easy and cost-effective implementation, high power levels thanks to the laser topology, increased resolution with respect to edge filter implementations thanks to the narrow laser linewidth and tunable sensitivity. The device exhibits temperature sensitivity due to the sensitivity of the FBG sensors and requires compensation by means of an identical dummy FBG. Therefore, the simplest configuration utilizes a 1×2 optical switch with two identical FBGs, one of them acting as a reference sensor. Multiple sensors may be interrogated using multiple-port optical switches. The cost of the optical switches increases with the number of ports, limiting the application of this topology to small-scale applications.

6. Patents

A patent is pending for the technique presented in this paper.

Author Contributions: Conceptualization, N.A.S., I.S., C.S. Methodology, software, formal analysis, investigation and writing—original draft preparation, N.A.S., C.L., I.S., C.S.; All authors have read and agreed to the published version of the manuscript.

Funding: This research received no external funding.

Data Availability Statement: Data presented in this work are available upon request.

Conflicts of Interest: The authors declare no conflicts of interest.

 doi:10.20944/preprints202404.0491.v1

Appendix A

The core refractive index of an EDF is a complex number with its imaginary part representing the gain (if it is positive) or the loss (if it is negative) of the signal (which is assumed within the ASE spectrum), while for the pumping wavelength it is always negative due to absorption of the pump from the Erbium ions [15,16]. It can be calculated through the state populations and the steady state equations for both wavelengths. Although the formalism described in [15,16] may be adopted, the ion cluster formation for heavily doped EDF, requires a modeling that includes the effects due to the interaction within ion pairs [17]. According to this model, the density of clustered ions is $N_c = mkN_t$ where N_t is the total ion density in the core, m is the number of ions in a cluster and mk is the percentage of ions in cluster form. Considering a two-level system, including the pair induced quenching (PIQ) of the clusters, the steady state solutions of the rate equations lead to [17]:

$$N_{c2} = N_c - N_{c1} = N_c \frac{R + W_{12}}{A_{21} + m(R + W_{12}) + W_{21}} \tag{A1}$$

$$N_{s2} = N_s - N_{s1} = N_s \frac{A_{21} + W_{21}}{A_{21} + R + W_{12} + W_{21}} \tag{A2}$$

where, N_s is the single ions density $(N_t - N_c)$, $N_2 = N_{s2} + N_{c2}$, $N_1 = N_t - N_2$ while the absorption and emission rates $W_{12}(\lambda_s)$, $W_{21}(\lambda_s)$ for the signal wavelength λ_s are given by the relations:

$$W_{12}(\lambda_s) = \frac{\lambda_s \sigma_{as}(\lambda_s) P(\lambda_s) \Gamma(\lambda_s)}{hc\pi b^2} \tag{A3}$$

$$W_{21}(\lambda_s) = \frac{\lambda_s \sigma_{es}(\lambda_s) P(\lambda_s) \Gamma(\lambda_s)}{hc\pi b^2} \tag{A4}$$

Moreover, the pump rate at λ_p=980nm is:

$$R(\lambda_p) = \frac{\lambda_p \sigma_{ap}(\lambda_p) P(\lambda_p) \Gamma(\lambda_p)}{hc\pi b^2} \tag{A5}$$

where h is the Plank's constant and for the signal wavelength λ_s=1534nm the emission and absorption cross sections are σ_{es} =3.24×10-25 and σ_{as} =3.69×10-25m2 respectively, while the absorption cross section for the pump wavelength is σ_{ap}=2×10-25 m2. Additionally, the overlap integrals are calculated as:

$$\Gamma(\lambda) = 1 - e^{-2[b/\omega(\lambda)]^2} \tag{A6}$$

with

$$\omega(\lambda) = a\left(A_1 + \frac{A_2}{V^{1.5}} + \frac{A_3}{V^6}\right) \tag{A7}$$

and $a = 5\mu$, $\frac{b}{a} = 1$, $V = \frac{2\pi a NA}{\lambda}$, $NA = 0.2$. Moreover, A1=0.616, A2=1.66, A3=0.987, the doping concentration N_t = 6.6×1025 ions/m3 and the spontaneous emission rate A21=1/0.0103 sec-1. Considering an input signal power $P(\lambda_s)$ and a pumping power $P(\lambda_p)$, the gain for the signal and the absorption of the pumping wavelength are given [15–18] respectively by:

$$G = 4.343\Gamma(\lambda_s)(\sigma_{es}N_2 - \sigma_{as}N_1) \ \ (dB/m) \tag{A8}$$

$$A = 4.343\Gamma(\lambda_p)(-\sigma_{ap}N_1) \ \ (dB/m) \tag{A9}$$

where, the involved value of k will be determined experimentally and m=2 ions per cluster. For the calculation of the gain of an EDF with length *L* and the remaining pump power at the end of it, a

Preprints.org (www.preprints.org) | NOT PEER-REVIEWED | Posted: 8 April 2024 doi:10.20944/preprints202404.0491.v1

numerical procedure should be applied. Particularly, we discretize the length L in small segments as depicted in Figure A1.

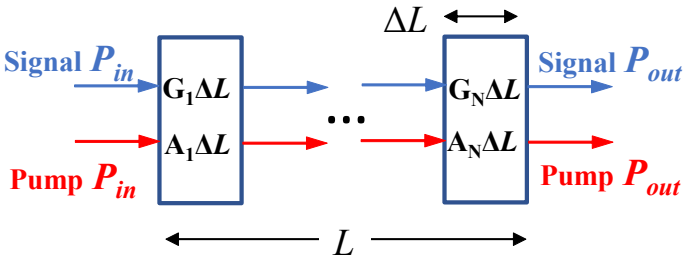

Figure A1. Segmentation of heavily doped EDF for gain and residual pumping calculation.

The length of each segment has been selected to be so short, that G and A may be considered constants throughout ΔL. For a heavily doped EDF, in the gain saturation range, each segment is characterized by different gain and pumping power. Using a recursive procedure both the residual pump power P_{out} and the final gain will be calculated by the signal ratio $\frac{P_{out}}{P_{in}}$. By a suitable experimental setup, the residual pumping power may be measured and through the aforementioned calculation scheme the input pumping power may be derived.

The proposed experimental setup is depicted in Figure A2 and may be used for the EDF's gain saturation region as well. In Figure A2 a broad band source has been used in combination with a circulator and an FBG centered at the signal wavelength λ_s. An Erbium Doped Fiber Amplifier (EDFA) device has been employed in order to amplify the signal wavelength λ_s at a level from -40dBm to -10dBm. Moreover, the pumping level for the EDF under test ranges from 70 to 100mW. For two levels of pumping power 75 and 95mW the gain is depicted in Figure A3, where the input signal changes from small signal ($P_{in}(\lambda_s)$=-40dBm) up to almost -10dBm.

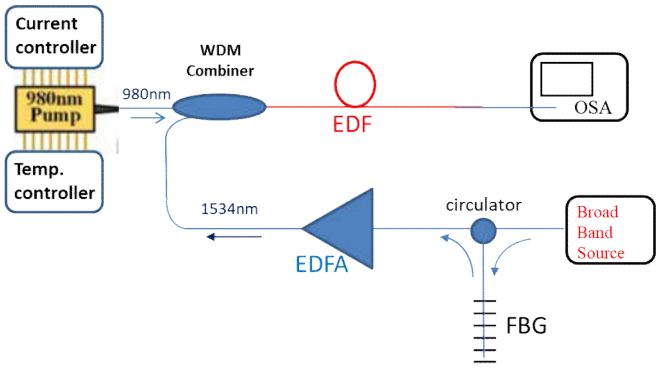

Figure A2. Experimental setup for the evaluation of the gain saturation versus the input signal power. The EDF is 47cm long and heavily Erbium doped.

Preprints.org (www.preprints.org) | NOT PEER-REVIEWED | Posted: 8 April 2024 doi:10.20944/preprints202404.0491.v1

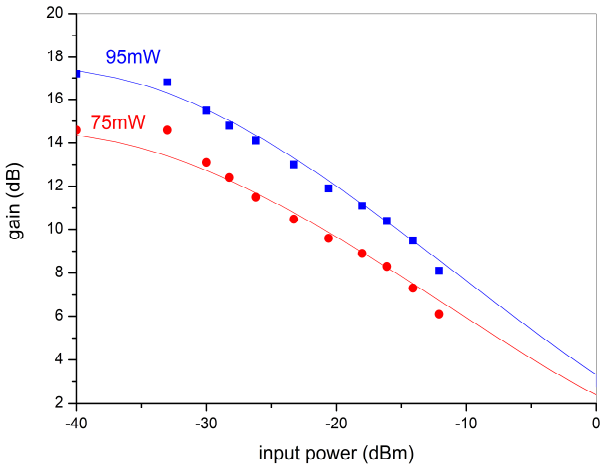

Figure A3. Experimental gain values (symbols) vs input signal power, for 95mW pumping power (blue symbols) and 75mW (red symbols). The fitted calculation curves for 95mW (blue solid line) and 75mW (red solid line) are depicted, according to the procedure described in the text.

Using the experimental values of Figure A3 we may calculate the small signal gain by applying (A8) and the segmentation calculation scheme by adjusting the value of k in order to coincide with the experimental ones. For the EDF of Figure A2's experimental setup, and the values depicted in Figure A3, the value of k is estimated to be 15.6% which is in the same order of the values referred to in the literature [20]. Moreover, the pumping power has been calculated from the measured power at the end of the EDF and the segmentation technique of Figure A1. Next, the curve of the saturation gain has to be determined.

The gain saturation vs input power signal is provided by the calculation scheme of the steady state PIQ equations, but this rather corresponds to the intrinsic parameters than the experimental conditions [19,22]. A similar drawback appears at the gain calculation through the saturation power parameter [18,21]. Nevertheless, the PIQ model incorporates the cluster-phenomenon and gives the potentiality to adjust the small signal gain according to the experimental results. On the other hand, the saturation parameter method provides the possibility to adjust the saturation according to the experimental conditions. Consequently, we adopted the PIQ model for the small signal gain and the estimation of k, but we had to follow the saturation parameter method for the approximation of the gain saturation vs the input power signal.

For the application of the saturation parameter method, we define the saturation power for signal and pump as follows [15]:

$$P_{sat}(\lambda_s) = \frac{hc\pi\omega_s^2 A_{21}}{\lambda_s(\sigma_{as} + \sigma_{es})} \tag{A10}$$

$$P_{sat}(\lambda_p) = \frac{hc\pi\omega_p^2 A_{21}}{\lambda_p \sigma_{ap}} \tag{A11}$$

where $\omega_s = \omega(\lambda_s)$ and $\omega_p = \omega(\lambda_p)$. By introducing the normalized saturation power for signal and pump respectively $p = \frac{P(\lambda_s)}{P_{sat}(\lambda_s)}$ and $q = \frac{P(\lambda_p)}{P_{sat}(\lambda_p)}$, the gain and absorption relations will be given as follows:

$$G = 4.343 N_t \frac{(q\sigma_{es} - \sigma_{as})}{1+q+p} \quad (dB/m) \tag{A12}$$

Preprints.org (www.preprints.org) | NOT PEER-REVIEWED | Posted: 8 April 2024 doi:10.20944/preprints202404.0491.v1

$$A = 4.343\,\frac{-\sigma_{ap}N_t}{1+q+p}\left(1+p\,\frac{\sigma_{es}}{\sigma_{as}+\sigma_{ap}}\right) \quad (dB/m) \qquad \text{(A13)}$$

In (A12) and (A13) the normalized field profile of the fundamental mode at the center of the core has been taken to be equal to one. Moreover, the small signal gain according to (A12), should coincide with the small signal gain derived by (A8). However, (A12) does not feature any parameter that may include the PIQ phenomenon and the potential adoption of *effective* cross-sections, in order to equate the small signal gains from both calculation schemes, is a tedious and controversial procedure. Instead, a rather reasonable approach is to follow the gain saturation response given by (A12), normalized to the small signal gain, while adjusting the saturation power in order to fit the experimental results. Particularly, by applying the segmentation procedure and reducing $P_{sat}(\lambda_s)$ accordingly (i.e. to approximately 7.5% of the maximum value), the gain saturation is scaled to the small signal gain provided by the PIQ method.

Following this method, the fitting curves have been derived, as it is depicted in FigureA3, for 47cm Er110 and for 75mW and 95mW pump power respectively. The saturation power is now approximately reduced to the 7.5% of its intrinsic value.

Next, we repeat the aforementioned procedure for a less doping-density EDF such as the Er30 fiber with N_t =2.1×10^{25} ions/m^3. The value of *k* is estimated now to be 9% while the $P_{sat}(\lambda_s)$ is reduced to 30% of its intrinsic value. Both parameters are reasonably differed from those of the Er110 fiber's, since the cluster – phenomenon is now mitigated whereas, the $P_{sat}(\lambda_s)$ is now closer to its maximum (i.e. intrinsic) value as anticipated [19,26].

In Figure A4 the experimental values for two pump powers are depicted, together with the corresponding fitting through the proposed model and for a 62cm EDF. Although the small signal gain is now less than that in the higher doped EDF, the saturation is pushed towards higher input power that consequently gives higher output power from the ring topology. Nevertheless, its loop losses should now be less in order to ignite the lasing operation.

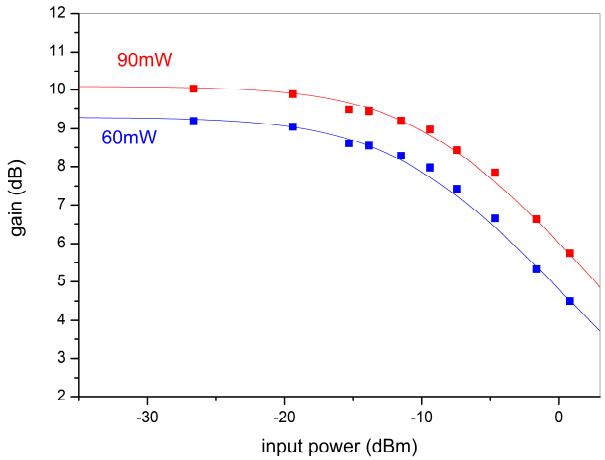

Figure A4. Experimental gain values (symbols) vs input signal power, for 90mW pump power (red symbols) and 60mW (blue symbols). The fitted calculation curves for 90mW (red solid line) and 60mW (blue solid line) are depicted, according to the procedure described in the text.

The proposed method is applied for a unidirectional ring EDFL, as that in Figure 1, with a circulator that forces the clockwise propagation direction. The output power is provided by the saturated gain vs input signal power as depicted in Figure A3. By determining the ring losses (i.e. the losses from the couplers and the reflectivity loss from the FBG) the input signal power should provide the required gain that will balance the losses and therefore corresponds to the output power. However, for higher output power or equivalently with less reflective FBG, a bidirectional

 doi:10.20944/preprints202404.0491.v1

operation may be adopted. The estimation of the output power for the bidirectional operation is rather more complicated, although its evaluation may be provided by a modified figure of merit.

References

1. Lopez-Higuera, J.M.; Rodriguez Cobo, L.; Quintela Incera, A.; Cobo, A. Fiber Optic Sensors in Structural Health Monitoring. J. Lightwave Technol. 2011, 29, 587–608. https://doi.org/10.1109/JLT.2011.2106479.
2. Tosi, D. Review and Analysis of Peak Tracking Techniques for Fiber Bragg Grating Sensors. Sensors 2017, 17, 2368. https://doi.org/10.3390/s17102368.
3. Grattan, K.T.V.; Sun, T. Fiber Optic Sensor Technology: An Overview. Sensors and Actuators A: Physical 2000, 82, 40–61. https://doi.org/10.1016/S0924-4247(99)00368-4.
4. Othonos, A.; Kalli, K. Fiber Bragg Gratings: Fundamentals and Applications in Telecommunications and Sensing; Artech House optoelectronics library; Artech House: Boston, Mass, 1999; ISBN 9780890063446.
5. Kashyap, R. Fiber Bragg Gratings; 2nd ed.; Academic Press: Burlington, MA, 2010; ISBN 9780123725790.
6. Shao, L.; Song, J.; Zhang, A.; He, S. Novel FBG Triangular Filter for Interrogating a FBG Sensor in Dynamic Strain Measurement. Optoelectr. Lett. 2006, 2, 336–338. https://doi.org/10.1007/BF03033516.
7. Kumar, S.; Ghorai, S.K.; Sengupta, S. Fiber Bragg Grating Sensor Interrogation Using Edge-Filtering with Long Period Grating Modulated Light Source. Opt Quant Electron 2023, 55, 847. https://doi.org/10.1007/s11082-023-05120-0.
8. Kieu, K.Q.; Mansuripur, M. Biconical Fiber Taper Sensors. IEEE Photon. Technol. Lett. 2006, 18, 2239–2241. https://doi.org/10.1109/LPT.2006.884742.
9. Bandyopadhyay, S.; Biswas, P.; Pal, A.; Bhadra, S.K.; Dasgupta, K. Empirical Relations for Design of Linear Edge Filters Using Apodized Linearly Chirped Fiber Bragg Grating. J. Lightwave Technol. 2008, 26, 3853–3859. https://doi.org/10.1109/JLT.2008.928192.
10. Romero, R.; Frazão, O.; Marques, P.V.S.; Salgado, H.M.; Santos, J.L. Fibre Bragg Grating Interrogation Technique Based on a Chirped Grating Written in an Erbium-Doped Fibre. Meas. Sci. Technol. 2003, 14, 1993–1997. https://doi.org/10.1088/0957-0233/14/11/018.
11. Yucel, M.; Koyuncu, O. Design and Implementation of a Passive Edge Filter with High Bandwidth and Slope. Micro & Optical Tech Letters 2019, 61, 2572–2578. https://doi.org/10.1002/mop.31923.
12. Tiwari, U.; Thyagarajan, K.; Shenoy, M.R.; Jain, S.C. EDF-Based Edge-Filter Interrogation Scheme for FBG Sensors. IEEE Sensors J. 2013, 13, 1315–1319. https://doi.org/10.1109/JSEN.2012.2235064.
13. Fiber Optic Sensors; Yu, F.T.S., Yin, S., Eds.; Optical engineering; Marcel Dekker: New York, 2002; ISBN 9780824707323.
14. Tanaka, S.; Ogawa, T.; Yokosuka, H.; Takahashi, N. Multiplexed Fiber Bragg Grating Vibration Sensor with Temperature Compensation Using Wavelength-Switchable Fiber Laser. Jpn. J. Appl. Phys. 2004, 43, 2969. https://doi.org/10.1143/JJAP.43.2969.
15. Sunanda; Sharma, E.K. Field Variational Analysis for Modal Gain in Erbium-Doped Fiber Amplifiers. J. Opt. Soc. Am. B 1999, 16, 1344. https://doi.org/10.1364/JOSAB.16.001344.
16. Stathopoulos, N.A.; Savaidis, S.P. Gain Calculation and Propagation Characteristics in Erbium-Doped Devices with Nonlinear Host Materials. Optics Communications 2008, 281, 80–89. https://doi.org/10.1016/j.optcom.2007.08.065.
17. Myslinski, P.; Nguyen, D.; Chrostowski, J. Effects of Concentration on the Performance of Erbium-Doped Fiber Amplifiers. J. Lightwave Technol. 1997, 15, 112–120. https://doi.org/10.1109/50.552118.
18. Giles, C.R.; Desurvire, E. Modeling Erbium-Doped Fiber Amplifiers. J. Lightwave Technol. 1991, 9, 271–283. https://doi.org/10.1109/50.65886.
19. Desurvire, E. Erbium-Doped Fiber Amplifiers: Principles and Applications; Wiley-Interscience: Hoboken, N.J, 2002; ISBN 9780471264347.
20. Teyo, T.C.; Leong, M.K.; Ahmad, H. Noise Characteristics of Erbium-Doped Fiber Amplifier with Optical Counter-Feedback. Jpn. J. Appl. Phys. 2002, 41, 2949–2950. https://doi.org/10.1143/JJAP.41.2949.
21. Bellemare, A.; Karbsek, M.; Riviere, C.; Babin, F.; Gang He; Roy, V.; Schinn, G.W. A Broadly Tunable Erbium-Doped Fiber Ring Laser: Experimentation and Modeling. IEEE J. Select. Topics Quantum Electron. 2001, 7, 22–29. https://doi.org/10.1109/2944.924005.
22. Durak, F.E.; Altuncu, A. The Effect of ASE Reinjection Configuration through FBGs on the Gain and Noise Figure Performance of L-Band EDFA. Optics Communications 2017, 386, 31–36. https://doi.org/10.1016/j.optcom.2016.11.009.
23. Stathopoulos, N.A.; Simos, I. Modelling of Non-Uniform and Fs-Laser Inscribed Fibre Bragg Gratings. Optical Fiber Technology 2022, 70, 102878. https://doi.org/10.1016/j.yofte.2022.102878.
24. Zhu, L.; Chen, Q.; Zhao, R.; Lou, X.; He, W. A Switchable Dual-Wavelength Erbium-Doped Fiber Laser Based on Saturable Absorber and Active Optical Fiber Ring Filter. Optoelectron. Lett. 2014, 10, 434–438. https://doi.org/10.1007/s11801-014-4166-8.

 doi:10.20944/preprints202404.0491.v1

25. He, W.; Zhu, L.; Dong, M.; Luo, F.; Chen, X. Stable and Tunable Narrow-Linewidth Erbium-Doped Fibre Laser Based on Polarization-Maintaining Fibre Ring Filter and PM-FBG. Laser Phys. 2014, 24, 125102. https://doi.org/10.1088/1054-660X/24/12/125102.
26. Saleh, A.A.M.; Jopson, R.M.; Evankow, J.D.; Aspell, J. Modeling of Gain in Erbium-Doped Fiber Amplifiers. IEEE Photon. Technol. Lett. 1990, 2, 714–717. https://doi.org/10.1109/68.60769.